Phase Diagram of the Nitric Acid/Water System: Implications for Polar Stratospheric Clouds

Keith D. Beyer* and Anne R. Hansen

Department of Chemistry, Wisconsin Lutheran College, Milwaukee, Wisconsin 53226

Received: January 24, 2002; In Final Form: June 6, 2002

We have investigated the HNO_3/H_2O binary liquid/solid phase diagram using a highly sensitive differential scanning calorimeter (DSC) and infrared spectroscopy of thin films. In particular we have sought to investigate the nitric acid trihydrate (NAT) and nitric acid dihydrate (NAD) regions. We report here a detailed stability region for NAD, including comment on the preferential freezing of NAD vs NAT. We have found metastability for NAD and pure HNO_3 outside of their normal thermodynamic stability. We have deciphered and more clearly defined the many eutectic transitions in the region of NAT, NAD, and nitric acid monohydrate (NAM). We also report a new solid phase mentioned previously in the literature that undergoes a transition at ∼228 K for samples in the range 54−75 wt % HNO_3. We have also detected other new phases that we deem either minor or not relevant for polar stratospheric clouds (PSCs). Finally, we have calculated the fraction of each solid that exists in a frozen sample on the basis of our measured enthalpies of fusion for the various solids. We compare our results to previous work on the nitric acid/water phase diagram, including recent work done on binary aerosols. The implications of our results for the freezing of nitric acid hydrates in PSCs are discussed.

Introduction

Polar stratospheric clouds (PSCs) play a crucial role in the depletion of ozone (O_3).[1,2] PSCs have been discussed in terms of three types: Ia (composed primarily of solid particles); Ib (liquid particles consisting of a ternary mixture of $HNO_3/H_2SO_4/H_2O$); II (water-ice).[3,4] In the case of type Ia, it is believed that nucleation of one or more solids in the ternary liquid particles occurs, which leads to condensation of background vapors on the particles at temperatures 2−4 K above the frost point of water ice. This leads these newly solid particles to grow to a size where they can sediment to lower regions in the stratosphere.[5−7] Laboratory experiments have shown this to be a possible mechanism,[8,9] and field measurements have shown solid particle formation is the most likely explanation for observations of very large particles.[10,11] It has been shown by various laboratory studies summarized by DeMore et al. that the surface reaction probability of stratospheric gases depends on the nature of the surface;[12] therefore, it is critical to know the phase diagrams of the various acid hydrates accurately.

Many investigators have studied the phase diagram of HNO_3/H_2O, determining the various hydrates that can form. The first studies were performed about a century ago.[13,14] However, the existence of nitric acid dihydrate (NAD) was not reported until recently (Ritzhaupt and Devlin,[15] Tolbert and Middlebrook[16] [IR spectra]; Ji and Petit[17] [DSC, liquid/solid phase diagram]; Worsnop et al.[18] [vapor pressure/vapor pressure phase diagram]). But even now there is still disagreement among the published work regarding the conditions of NAD stability.[17−20] NAD is an important hydrate because it has been seen to form preferentially to NAT in laboratory experiments under stratospheric conditions.[18,19]

Experiments have been performed by studying aerosols composed of HNO_3/H_2O with compositions representative of those expected for stratospheric droplets. These experiments have sought to elucidate the solid phase(s) that nucleate in stratospheric aerosols under winter polar stratospheric conditions. In experiments where aerosols have been studied at stratospheric temperatures, a significant limitation is time of observation. For aerosols with ∼54 wt % HNO_3 composition (NAT) no nucleation is seen in the aerosols on the time scale of hours (though at higher concentrations, ∼NAD composition, nucleation is seen).[21] In other experiments, temperatures significantly below those in the stratosphere are used to induce nucleation on the short time scale of the experiment (tens of seconds to minutes).[22−25] However, it is not conclusive that the solids formed at these lower temperatures are the same as would form at higher temperatures representative of the stratosphere. Recently, studies have been reported on very small samples in contact with a hydrophobic surface where nucleation was detected.[26,27] In these studies the temperature was dropped until all the samples either froze or no more nucleation was detected (190−160 K). The samples were then warmed, and the phases present were determined by the visually observed melting points. However, this type of study requires very accurate knowledge of the melting and various phase transition temperatures.

In this paper we present results of our investigation of the liquid/solid binary phase diagram of aqueous nitric acid. We have investigated and mapped the stability region of NAD in addition to better explaining the stability region of several nitric acid hydrates including a comprehensive determination of the various eutectic temperatures.

Experimental Section

Sample Preparation. Acid samples were prepared by diluting 68.5 wt % ACS reagent grade HNO_3 supplied by either Fischer or Aldrich with Culligan-purified water. Samples above 68.5 wt % were diluted from 90 wt % ACS reagent grade HNO_3. The concentrated acid was standardized by acid−base titration, and the concentration of all samples is known to ±0.40 wt %.

* Corresponding author. E-mail: Keith_Beyer@wlc.edu.

10.1021/jp025535o CCC: $22.00
Published on Web 10/02/2002

Infrared Spectra. The sample cell used for infrared spectra is shown schematically and explained in detail in previous literature.[28] Briefly, a small drop of HNO_3 solution was placed between two AgCl windows, which were held in the center of an aluminum block by a threaded metal ring. Sample volumes were either 5−8 μL or ∼0.1 μL. On each side of the aluminum block a Pyrex cell was purged with dry nitrogen gas. KBr windows were placed on the end of each cell, sealed with O-rings, and held in place by metal clamps. Heat tape was wrapped around the purge cells to prevent condensation on the KBr windows. The sample was cooled by immersing the end of the aluminum block in liquid nitrogen and warmed by resistive heaters connected to a temperature controller. Temperature was measured by a copper/constantan thermocouple placed at the edge of the AgCl windows and connected to the temperature controller. The temperature of the cell was calibrated using Culligan-purified water and high-purity organic solvents (Aldrich): decane, octane, and acetic anhydride, of which the melting points are 243.5, 216.4, and 200.2 K, respectively.[29] The IR cell temperatures are known on average to within ±1.3 K of the transition temperatures measured with the DSC.

Spectra were obtained with a Mattson Instruments Galaxy 4020 FTIR with 16 cm^{-1} resolution. Each spectrum is the average of four scans. Before spectra were taken of a sample, a reference scan was obtained from a dry, purged sample cell. Samples were cooled to 192 K at 3 K/min and then allowed to warm to room temperature without resistive heating, typically this was ∼1 K/min. If acid samples did not freeze during cooling, they were held at ∼145 K for up to 1 h and the samples would crystallize upon warming. In all cases our spectra compare well for ice, β-NAT, NAD, and NAM with those previously published.[15,30]

Differential Scanning Calorimeter. Thermal data were obtained with a Mettler Toledo DSC 822e with liquid nitrogen cooling. Industrial grade nitrogen gas was used as a purge gas with a flow rate of 50.0 mL/min. The temperature reproducibility of this instrument is better than ±0.05 K. Our accuracy is estimated to be ±0.9 K with a probability of 0.94 on the basis of a three-point temperature calibration[31] using indium, HPLC grade water, and anhydrous, high-purity (99%+) octane from Aldrich, the latter two stored under nitrogen. The sensitivity of our instrument to thermal signals is high. For example, one of the weakest transitions we detect is the eutectic melting of HNO_3 at 205 K (which is far away from other, possibly interfering transitions); it has the lowest energy per mass of any solid (except ice) in this system. In an experiment where the signal was near our detection limit, we measured a signal of 0.17 mJ for a sample that had a total mass of 21.798 mg. Using the known enthalpy of fusion for HNO_3,[32] we calculate the mass fraction of the sample that is solid HNO_3 to be 4.7×10^{-5} or 47 ppm. Our signal-to-noise ratio is 1.8, which is taken to be the integrated energy of the signal divided by the integrated energy of the largest noise peak.

Samples were contained in a 30 μL platinum pan and typically had a mass of ∼22 mg, though some samples were very small (∼1 mg), to see if there were any effects on the phase transitions due to sample size (we saw none). Each sample was weighed before and after the experiment using a Mettler-Toledo AT20 microgram balance. The average mass loss from evaporation during the experiment was less than 2%. A typical sample was cooled to 183 K at 10 K/min, held at that temperature for 5 min, warmed to 203 K at 10 K/min, and then warmed at a slower heating rate of 1 K/min until 298 K.

A study of the effect of scan rate on melting temperatures was also performed. In this case samples of 25.0 wt % HNO_3 were cooled at 10 K/min to 138 K, held for 5 min, then warmed to 298 K at 0.5, 1, 2.5, 5, and 10 K/min in separate experiments. Three trials were performed at each scan rate, and the experimentally determined melting points averaged for each rate.

Results

Scan Rate. Melting is an endothermic process and DSC instruments measure the difference in heat flow between a sample and a reference, thereby generating a thermogram showing this difference. Initial deflection of the thermogram from baseline (onset of melting) depends on the heating rate of the instrument, but these effects are compensated for with a calibration method and thereby do not account for deviation among experiments run at different scanning rates. However, a second significant feature of thermograms is the peak temperature (the temperature at which melting has completed). The peak temperature is also a function of scanning rate; however, this cannot be compensated for with standard corrections. Therefore, we undertook a study of scanning rate on the peak temperature for a sample of 25.0 wt % HNO_3 similar in nature to that done by Chang et al.[33] for cooling samples. Figure 1 shows typical thermograms for the 25.0 wt % solutions warmed at various rates (see figure caption.) For a sample of this concentration we see two peaks. The first peak is for the melting of NAT at the ice/NAT eutectic of 230.6 K. As the sample is warmed, the ice slowly melts until the equilibrium melting point is reached at ∼245 K when any remaining ice finally melts, resulting in the second peak in the thermogram. As is readily evident, the onset temperatures of the eutectic melting peak are the same, but the peak temperatures of both the eutectic and final melting transitions vary with scanning rate. For eutectic transitions, we record the onset temperature, but for final melting of a phase, we record the peak temperature. The average peak temperature of three runs at each scan rate was plotted, and it was found that the relationship was linear (these temperatures are plotted on the phase diagram in Figure 2, with the scan rate for each point labeled). Thus the peak temperature at a theoretical scan rate of 0 deg/min was calculated to be 244.27 K. Our value for a scan rate of 1 deg/min is 244.81 K, which is a difference of 0.54 K. This value is within the estimated error of our instrument, therefore a warming rate of 1 deg/min was used for all samples.

Phase Diagram. Samples were cooled to a minimum temperature of 183 K, a typical low temperature in the winter polar stratosphere. Samples cooled to this temperature should produce the phases expected in stratospheric aerosols if the aerosols freeze. Figure 2 shows the phase diagram of nitric acid and water with the following data plotted: historic data of Pickering,[13] Kuster and Kreman,[14] and Potier and Potier.[34] We have also plotted the data of Ji and Petit[17] along with our data. It is seen that our data are in agreement with the historical work for nearly all concentrations. Exceptions are our melting points for solutions near the NAT exact composition (53.8 wt %), where our data are higher than the historical work. It is worth noting that the data of Ji and Petit for the NAT stability region generally show lower melting points than the historical or our work. They did not give a comparison of their work to the historic data, so we do not have an explanation for the difference. In Figure 3 we have expanded the region of the phase diagram between 54 and 84 wt % (the area of NAT, NAD, and nitric acid monohydrate (NAM) stability). We clearly have several transitions occurring between 227 and 234 K and will discuss

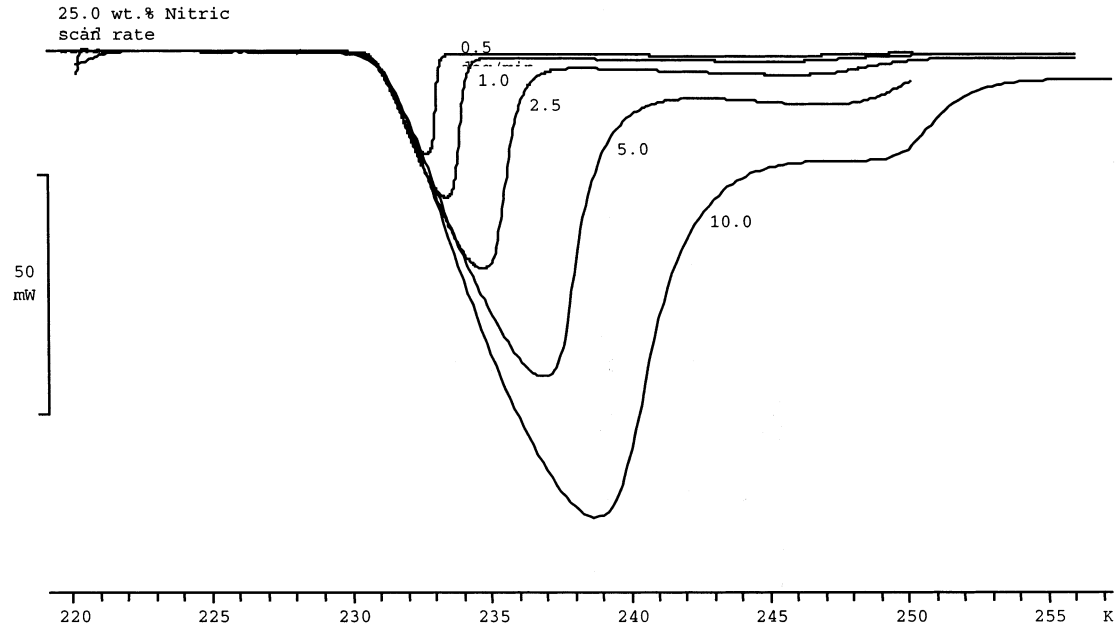

Figure 1. Thermograms showing heating of 25.0 wt % nitric acid samples at heating rates of 0.5, 1, 2.5, 5, and 10 deg/min. In this case, the peak temperature of interest is that of the second peak, which corresponds to the final melting of ice in the sample.

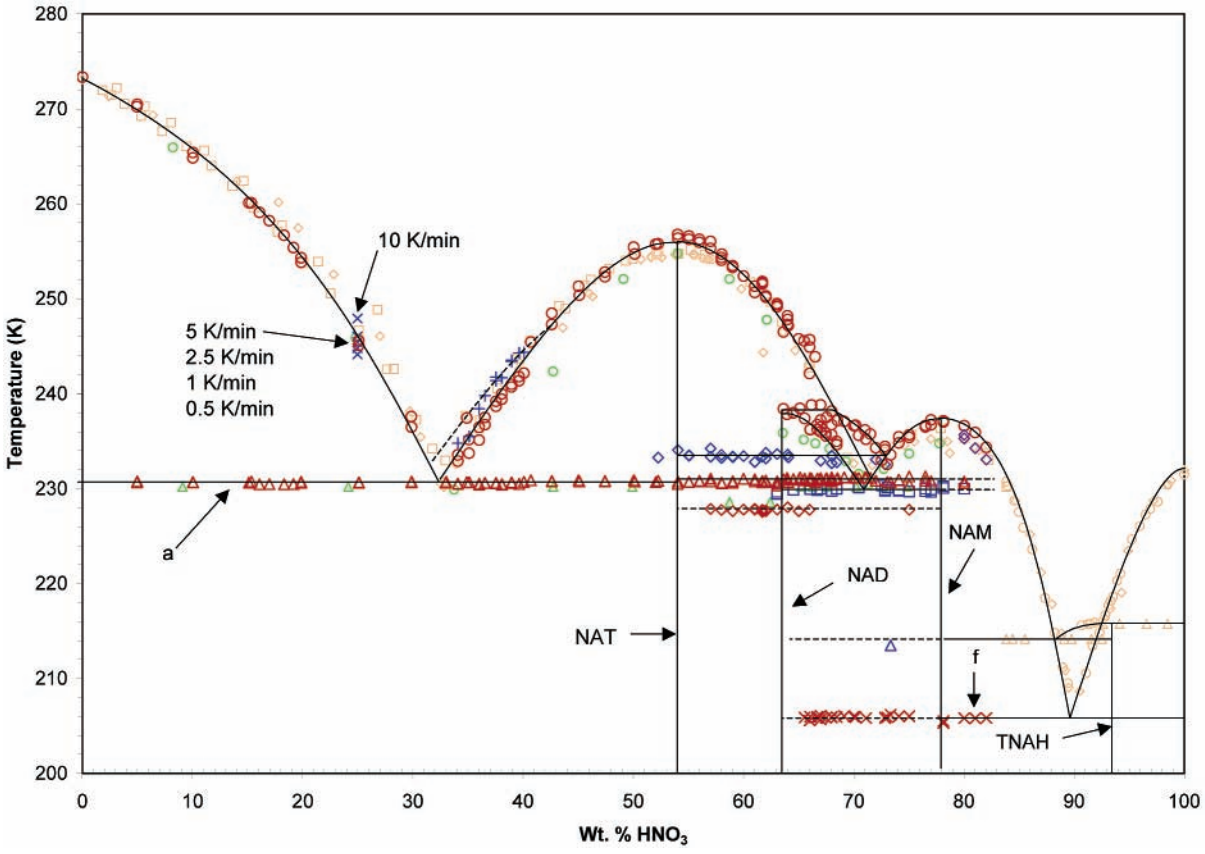

Figure 2. Phase diagram of the binary system nitric acid/water. Letters correspond to areas indicated in text and Table 1; lines drawn on the phase diagram serve as guides only. Historic data (gold): squares, Pickering; diamonds, Kuster and Kreman; circles and triangles, Potier and Potier. Light green symbols are those of Ji and Petit, circles are final melting, and triangles are eutectic melting. Our data: red circles, final melting; red triangles, ice/NAT and NAT/NAM eutectic melting; blue ×'s, scan rate experiment data; blue pluses, additional NAT transition (see text); blue diamonds, NAD transition (see text); blue squares, NAD/NAM eutectic; red diamonds, TNAN melting (see text); purple diamonds, new NAM transition (see text); blue triangle, TNAH (see text); red ×'s, NAM/HNO_3 eutectic.

their identity in detail below. A summary of all eutectic transitions is given in Table 1.

Water/NAT Eutectic. This eutectic spans the composition range below 53.8 wt % HNO_3. The average temperature of all samples is 230.64 ± 0.13 K (line a in Figure 2). Our data correlate well with that of Ji and Petit.[17]

Ice Melting/NAT Melting. The upper data points in the region between 0 and 33 wt % HNO_3 correspond to the melting

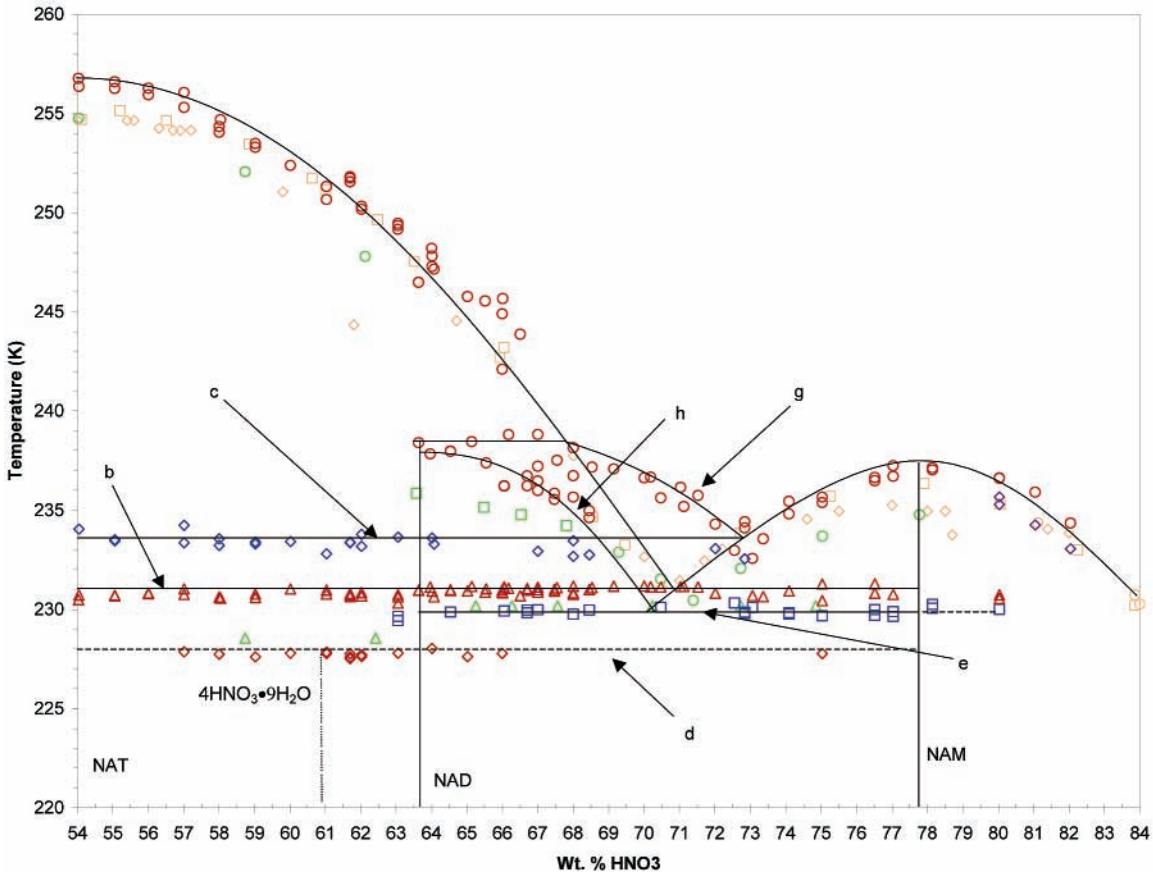

Figure 3. Expanded view of the nitric acid/water phase diagram for region of NAT, NAD and NAM stability. Letters correspond to areas indicated in text and Table 1, lines drawn on the phase diagram serve as guides only. Historic data (gold): squares, Pickering; diamonds, Kuster and Kreman. Light green symbols are those of Ji and Petit, circles are final melting, triangles are eutectic melting, and squares are NAD melting. Our data: red circles, final melting; red triangles, ice/NAT and NAT/NAM eutectic melting; blue diamonds, NAD transition (see text); blue squares, NAD/NAM eutectic; red diamonds, TNAN melting (see text); purple diamonds, new NAM transition (see text).

TABLE 1: Summary of Transitions in Nitric Acid/Water Binary System

area in Figures 2 and 3	transition	temp (K)	concn range (wt % HNO_3)
a	H_2O/NAT Eutectic	230.64 ± 0.13	5−52
b	NAT/NAM Eutectic	230.89 ± 0.25	54−80
c	NAD "Transition"	233.33 ± 0.40	52−73
d	$4HNO_3•9H_2O$ (TNAN)	227.76 ± 0.12	57−75
e	NAD/NAM Eutectic	229.92 ± 0.18	64.5−80
f	NAM/HNO_3 Eutectic	205.85 ± 0.18	65.5−82

of ice in contact with aqueous HNO_3. Our melting points correspond quite well with the historic data and Ji and Petit.[17] From 33 wt % to the NAT stoichiometric composition of 53.8 wt %, the upper data represent the melting of NAT in contact with aqueous HNO_3 solution. In our IR experiments, samples were studied with concentrations between 45 and 56 wt % HNO_3, and in all cases the major phase seen was β-NAT from comparison with reference spectra.[30] Two features are noteworthy in this region of the phase diagram. First, our melting points near the pure NAT melting region are at a higher temperature than either the historic data or that of Ji and Petit. A reasonable explanation for our difference with the historic work is simply experimental technique; they observed final melting with the naked eye, whereas we used a highly sensitive thermal instrument. It can be deduced that their observations (of a lack of solid in solution) were obtained at temperatures that were too low. The difference is not large (at most 2 K at the peak); however, it does not fall within the error of our experiment, and thus we feel it is a real difference. Also, note that the NAT melting temperatures of Ji and Petit are in general lower than the historic data (by as much as 5 K). However, at the NAT stoichiometric peak, their data agree with the historic data, thus also indicating that the historic data at this point may be too low.

A feature we have observed in the low concentration NAT region is an additional, very small transition between 33 and ~40 wt % HNO_3. Because the total energy measured accompanying this transition is very small (on the order of ~10 millijoules per gram of sample), and we have not seen anomalous signatures in the IR, the mass in this phase must also be quite small. Therefore, we do not consider it significant for stratospheric chemistry. However, the transition is apparent in our thermograms and thus we have reported it. Another interesting feature of this transition is that some of the melting points from the historic work correspond to the melting temperatures of this small phase (i.e., the 35 wt % sample). We have not seen any evidence for the higher hydrates indicated by Pickering[13] (HNO_3·$18H_2O$ = 18 wt %) or Worsnop et al.[18] (HNO_3·$10H_2O$ = 26 wt %), though we performed experiments on samples at 1 wt % intervals between 15 and 20 wt % and have multiple samples at 25 wt % (see Figure 2). Indeed, if the transition we have identified does correspond to the melting of a new hydrate, its concentration would be at least ~41 wt % HNO_3, which is where the curve we have drawn crosses the NAT freezing envelope (peritectic point).

NAT/NAM Eutectic. This eutectic at 230.89 ± 0.25 K (average of samples with transition, line b in Figure 3) between

54 and 80 wt % nitric acid is the eutectic melting of NAT/NAM. Our assignment of this transition is due to the fact that the temperature of this transition holds constant through the range of composition from pure NAT to pure NAM. Also, the size of the eutectic melting peak in the DSC thermogram fits the trend that there should be a very small eutectic peak at the pure composition of both solids, and a large peak at the eutectic composition (~71 wt %). Were this a transition due to a eutectic between NAT and NAD, the transition energy should peak at a composition between pure NAT and pure NAD and disappear in solutions with concentrations higher than pure NAD. This is not seen to be the case. Also, it is clear that there must be a NAT/NAM eutectic that spans the entire range of concentrations, and the transitions at 230.89 K meet that criterion. Additionally, a transition is seen at ~233 K appearing in solutions above 52 wt %, which we have assigned to NAD for reasons discussed below.

NAD Transition. All samples ranging from 58 to 64 wt % that were examined by infrared spectroscopy and determined to be exclusively NAD melted at ~233 K. The average temperature of this transition in DSC samples in the range 52−73 wt % HNO_3 was 233.33 ± 0.40 K (line c in Figure 3). In all cases but two (72 and 73 wt %), samples with a transition at 233 K also had a final melting corresponding to the NAT envelope. As can be seen from Figure 3, a line drawn through these points and continuing to higher concentration intersects the NAM and NAD melting envelopes (discussed below), making this a eutectic line. On the basis of our results, we assign the 233 K transition to a melting of NAD. However, we must note, this assignment does not seem to fit standard thermodynamic theory. As stated, the transition temperature corresponds to the intersection of the NAD and NAM melting envelopes (Figure 3), indicating a eutectic melting of NAM in contact with NAD. However, at the lower concentrations (<63 wt %) NAM has already melted at the NAT/NAM eutectic of ~231 K. Additionally, the tie line for the eutectic should only extend from the intersection of the melting envelopes to the NAD exact composition (63.6 wt %); these transitions are occurring at lower concentrations. It is also unlikely that these transitions correspond to a melting envelope *curve*; the transition temperatures are very close together over a significant range of concentrations with little to no curvature. Therefore we do not have a thermodynamic explanation for this transition other than that it is a melting of NAD in coexistence with NAT. This transition temperature was used as evidence for the existence of NAD in droplet studies using a microscope, as reported by Salcedo et al.[26,27] However, as evidence for NAD, they report melting temperatures between 231 and 234 K. We have assigned the transition at 231 K as the NAT/NAM eutectic melting temperature, which, in their studies would correspond to the melting of NAM in contact with NAT rather than a melting of NAD. This would seem to cast some question on their results for the nucleation rates of NAD, if they are including samples that have a melting transition due to NAM (231 K) without a transition due to NAD (234 K).

NAD Melting Envelope. In the expanded view of Figure 3, it can easily be seen that there is a melting envelope between 68 and 73 wt % HNO_3 (curve g) that does not correspond to the NAT or NAM melting envelopes. Infrared spectra of these samples corresponded to either NAD or a mixture of NAD and NAM prior to complete melting. Also, melting transitions were seen in the DSC along a line ~239 K between 64 and 68 wt %. Clearly there is a peritectic point at the intersection of the melting envelope and the 239 K melting line. Finally, the point of intersection of the melting envelope and the NAM melting envelope corresponds to the NAD transition at 233 K described above. As noted above, however, samples more concentrated than 63.6 wt % that had a transition at 233 K had final melting transitions that correlated with the NAT melting envelope (72 and 73 wt % samples were exceptions). Clearly, this indicates that NAD melts at 233 K in the presence of NAT, but at a higher melting envelope when NAT is lacking. Therefore, we assign the melting envelope indicated as curve g in Figure 3 to NAD. This envelope is at a much higher temperature than that assigned by Ji and Petit[17] (about 5 K higher). The work of Worsnop et al.[18] placed the NAD stability region much below the NAT and NAM melting envelopes: the highest temperature for NAD existence was reported as ~212 K before it underwent a solid−solid-phase transition converting to NAT. There is a transition at 213−214 K that corresponds to the eutectic melting of NAM in the presence of tetrakis(nitric acid) hydrate (TNAH, $4HNO_3 \cdot H_2O$), as first identified by Potier and Potier.[34] As can be seen in Figure 2, we had one sample (73.4 wt %) that showed this transition, but there were others in experiments where samples were cooled to 138 K and then warmed, which are not analyzed in this paper. The transitions we observed occurred both outside and inside the thermodynamic stability region, and therefore it is possible this is the transition seen by Worsnop et al. rather than a NAD transition.

We have also observed a number of melting transitions at lower temperatures than the upper melting envelope for the same range of concentrations. We have drawn a curve through these data on the phase diagram (curve h in Figure 3). As can be seen, we have drawn this curve to intersect with the NAM melting envelope, though we have no corresponding data between 68.5 wt % HNO_3 and the curve intersection with NAM at ~70 wt %. We do not have an explanation for why there are two curves that seem to correspond to NAD melting in both cases, other than the possibility that there are two crystal structures of NAD with one being slightly more stable than the other. However, we have no evidence from our IR experiments that would support such a conclusion.

NAD/NAM Eutectic. The transition at 229.92 ± 0.18 K (average of samples, line e in Figure 3) we have assigned to the eutectic melting of NAD/NAM. Our assignment is based on the observation that all samples with concentrations lower than 78 wt % that displayed this eutectic also had a final melting transition corresponding to the melting envelopes we have assigned to NAD (lower curve described above, curve h in Figure 3) or NAM, respectively.

New Low-Temperature Phase. We have identified a unique transition at 227.76 ± 0.12 K (average of samples with transition, line d in Figure 3). As can be seen, we find a range of samples that undergo this transition (57−66 and one at 75 wt %). This low-temperature transition was seen by Ji and Petit[17] and described simply as a "metastable invariant". Salcedo et al.[27] saw transitions between 224 and 228 K in microscopic droplets of composition 54 wt % HNO_3 in contact with a hydrophobic surface. However, they interpreted these transitions as the melting of NAD. In our work, the transition is an endotherm and therefore corresponds to a melting. This transition is not a solid−solid phase transition because in all cases the endotherm was immediately followed by an exotherm, thus indicating a melt−recrystallization paired transition (see Figure 4 for a sample thermogram). We have identified a unique peak in the infrared that correlates with the transition temperatures of this solid in the DSC. Figure 5 shows a comparison of spectra of NAD and the new solid. As can be readily seen, the spectra

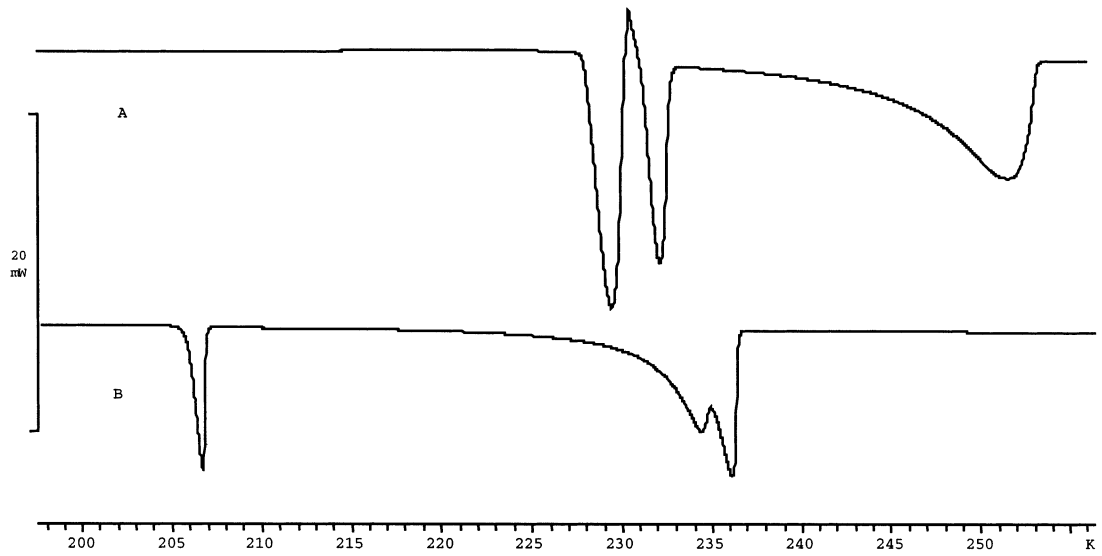

Figure 4. DSC thermograms of 61.03 wt % (A) and 81.04 wt % HNO_3 (B) solutions taken with a Mettler-Toledo 822e instrument. Exotherms occur above the baseline. In sample A the first peak is due to the melting of TNAN, which then recrystallizes (peak above the baseline) and then is immediately followed by the eutectic melting of NAD, and finally the melting of NAT. In sample B, the first peak is the eutectic melting of solid HNO_3 at ~206 K, followed by the new transition at ~234 K and the NAM melting at 236 K.

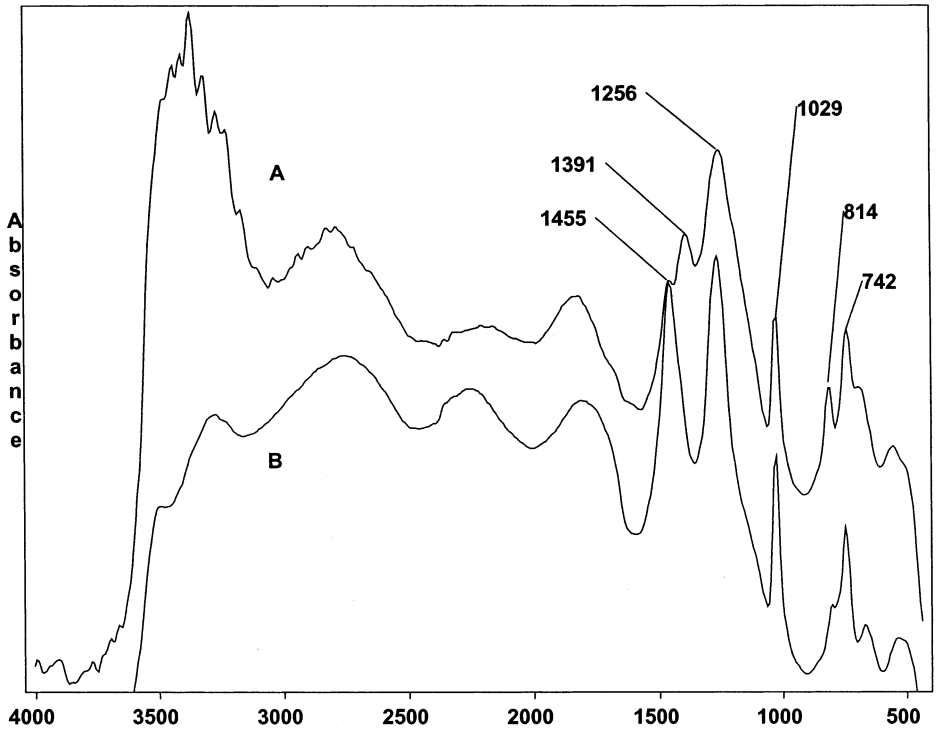

Figure 5. Infrared spectra of thin films showing TNAN (spectrum A) produced from a 63.0 wt % sample and NAD (spectrum B) produced from a 63.6 wt % sample.

are nearly identical except for a unique peak at 1391 cm^{-1} for the new solid. We have assigned this solid a crystal composition of $4HNO_3 \cdot 9H_2O$ (tetrakis(nitric acid) nonahydrate, TNAN) on the basis of the following evidence: (1) The sample with the largest peak area in the DSC for the ~228 K transition (thus greatest fraction of sample in this phase) was 61.03 wt % HNO_3. A composition of $4HNO_3 \cdot 9H_2O$ has a weight percent of 60.87. (2) We would expect the IR spectra of TNAN to be very similar to that of NAD, because the crystal would only differ by one water molecule from that of NAD. This is seen to be the case upon comparison of the IR spectra. (3) We have also observed transitions in the IR where NAD formed first upon freezing of the sample and later converted to TNAN. This would clearly indicate that some type of crystal re-ordering occurred with a final composition near that of NAD. (4) Solutions that formed TNAN had subsequent transitions at 231 K (NAT/NAM eutectic), 233 K (NAD transition), and a final melting of NAT. Thus this is not simply another eutectic transition of known phases. (5) It is unlikely this transition corresponds to a metastable structure of NAD that converts to a more stable form at 228 K. Such a transition would be a solid−solid phase transition and only one peak would be seen in the DSC thermogram corresponding to the difference in fusion energies of the two crystal forms. We clearly observe a melt−recrystallization transition for all samples. (6) The nitric acid/water system has other fractional hydrates ($HNO_3 \cdot {}^1/_4H_2O$) and other metastable solids (α-NAT at low temperatures). Thus it is not unreasonable for other fractional or metastable hydrates to exist.

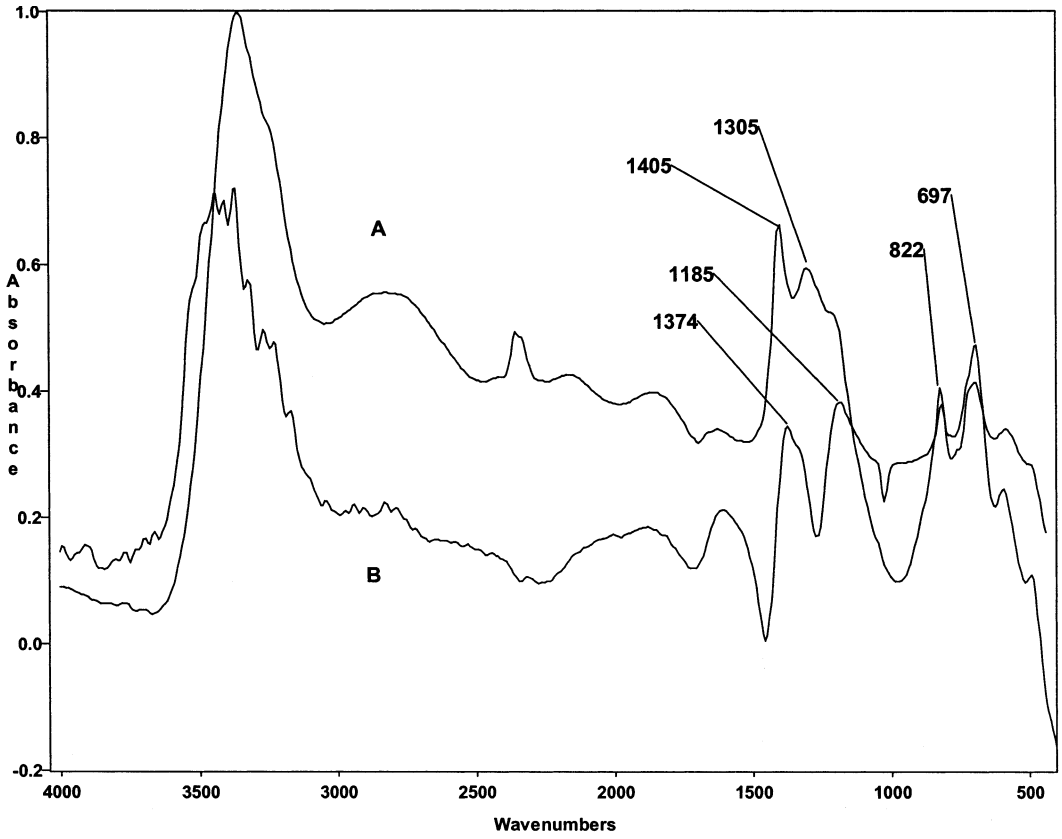

Figure 6. Infrared spectra of thin films showing β-NAT (spectrum A) produced from a 60.0 wt % sample and the spectrum resulting (spectrum B) from subtracting the NAD spectrum from the TNAN spectrum in Figure 5.

However, after listing these reasons, it must be stated that without conclusive evidence of the crystal structure, we cannot definitively assign the solid a specific composition, but we believe $4HNO_3 \cdot 9H_2O$ is plausible.

Prenni et al.[21] and Barton et al.[22] report spectra of "water-rich" NAD. However, the spectra of these authors are not in agreement with ours. The spectra presented as water rich NAD by Barton et al. have many differences from our spectra. In particular, they observed peaks at 1118 and 3430 cm^{-1} that we do not have in our spectra. They show a small peak at 1398 cm^{-1} that is near our peak at 1391 cm^{-1}, but our peak is stronger than the NAD peak at 1455 cm^{-1} (see Figure 5) whereas theirs is much weaker. They explain their spectra as being NAD mixed with α-NAT, which is especially apparent upon subtraction of a NAD spectrum from their water-rich NAD spectrum. We have performed the same subtraction with our spectra, and the results are given in Figure 6 along with our typical spectrum for β-NAT (we have temperatures too warm to form α-NAT and only see the β form; therefore we can only compare to β-NAT.) As can be seen in the figure, there are some similarities in the spectra. The peaks at 697 and 822 cm^{-1} are coincident, though not the same in shape. The subtraction of NAD from TNAN does leave a small peak at 1374 cm^{-1}, but this does not compare favorably to the β-NAT peaks at 1405 and 1305 cm^{-1}. Also, the subtracted spectrum has a minimum at 1305 cm^{-1} where β-NAT shows a peak. Our TNAN spectra are much closer qualitatively to that of Prenni et al. We see the same enhancement of the OH stretch at 2800−2500 cm^{-1}. However, they have no hint of a peak at 1391 cm^{-1} as our spectra show. They also state that, in general, the NAD features are less intense in their water-rich spectra. However, as is seen in Figure 5, our "NAD" peaks in the TNAN spectrum are as intense as they are in the pure NAD spectrum. Finally, phases that are simply "rich" or enhanced in one component do not demonstrate a thermodynamic transition unique from the nonenhanced phase, as we have seen in our DSC experiments. Therefore we conclude that the phase we identify as "TNAN" is not simply a mixture of NAD and NAT, or a "water-rich" NAD phase, but indeed is a new thermodynamic phase not previously identified. This conclusion has implications for the interpretation of the work of Salcedo et al.[27] who interpreted their transitions at 224−228 K to be NAD.

NAM Melting Envelope. As seen in Figures 2 and 3, our data for the melting of NAM correspond well with the historic data, though the exact NAM composition melting point is slightly high. We again observe that the melting temperatures of Ji and Petit[17] are low when compared to the historic and our data. We have also seen a new transition on the nitric acid-rich side of the melting envelope indicated by the purple diamonds in Figures 2 and 3. These new transitions are much stronger than the new, very weak transitions seen on the water-rich side of the NAT melting envelope. A typical thermogram is given in Figure 4 for a sample with this transition, and it can be seen that the energy of the transition is comparable to that of melting NAM. This would indicate (assuming energies of transition per gram are comparable) that there is a comparable amount of both NAM and this new phase in the samples.

Pure HNO_3 and TNAH. Referring to Figure 2, we have detected small amounts of pure nitric acid solid in most of the samples between 65 and 78 wt %. In addition, one sample in this range contained the tetrakis(nitric acid) hydrate (TNAH) first identified by Potier and Potier.[34] Though it may not be intuitively obvious that these samples should contain some amount of pure nitric acid solid (indeed, the range 65−78 wt % is outside the HNO_3 stability region), solutions with composition other than the exact composition of known solids will either have excess water or nitric acid in solution when the known solids form. Therefore, we should expect to see very small amounts of the pure HNO_3 solid present upon freezing of the

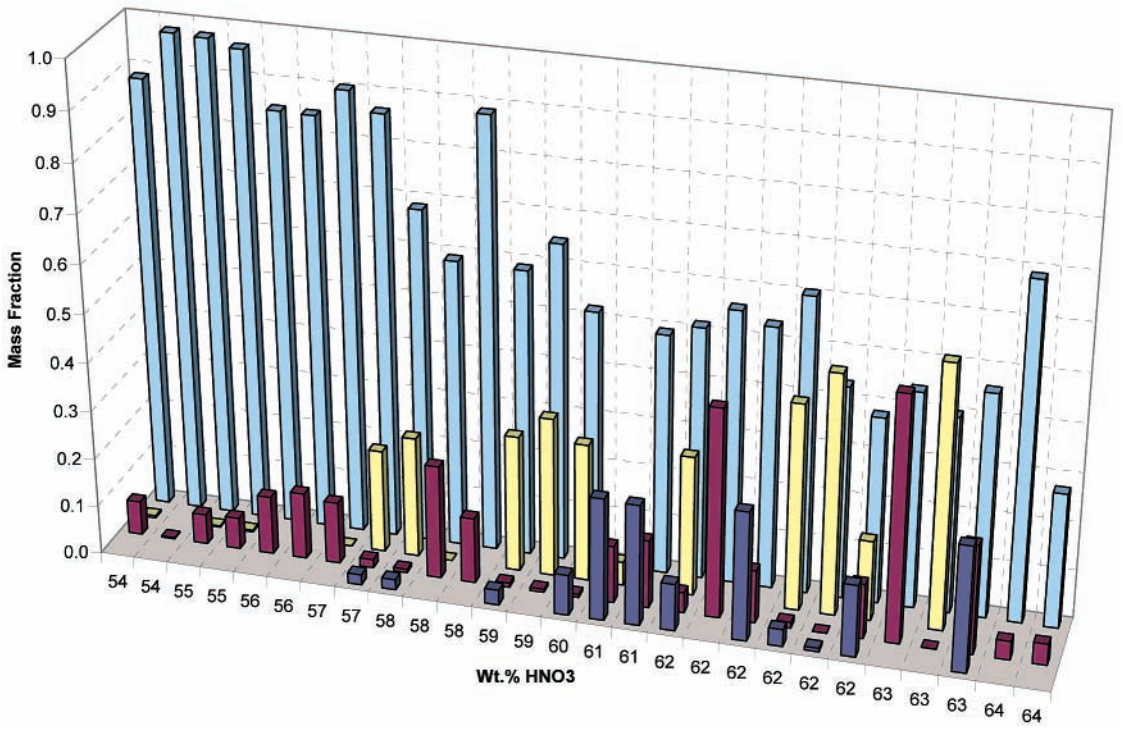

Figure 7. Fraction of each phase in DSC samples by mass: light blue, NAT; yellow, NAD; maroon, NAM; dark blue, TNAN. Data are organized by sample: each value on the *x* axis corresponds to an individual nitric acid sample with the concentration indicated.

TABLE 2: Summary of Molar Enthalpies of Fusion

	ΔH_{fus} (kJ/mol)	reference value
NAT	29.18 ± 0.80	29.10 ± 0.02[a]
NAD	20.02 ± 0.41	20.15[b]
NAM	17.66 ± 0.47	17.51 ± 0.01[a]

[a] Reference 32. [b] Wooldridge et al.;[41] no error estimation was given.

entire solution, and this is the case in our experiments. Probably the most interesting observation is that nitric acid does freeze as a pure solid rather than remaining liquid at the minimum temperature of our experiment (183 K). This is only 23 K below the NAM/HNO_3 eutectic temperature. The melting transitions we observed for pure HNO_3 were very small in the range 64−77 wt % HNO_3, corresponding to at most a very small fraction of the total sample (∼100 ppm at 64 wt % to ∼1000 ppm at 77 wt %).

Enthalpies of Fusion. Using the method described by Forsythe and Giauque,[32] we calculated the enthalpies of fusion for NAT, NAD, and NAM from our DSC data. Results are given in Table 2 along with comparison of literature data. It is seen that our data are in excellent agreement with previous work. We were unable to calculate the enthalpy of fusion for TNAN because in all cases melting transitions were occurring concurrent with recrystallization. Thus the melting and crystallization signals could not be separated.

Fractions of Each Hydrate in the Solid Phase. Using the fusion enthalpy values we measured (described above) and assuming the fusion enthalpy of TNAN can be approximated as the same as that for NAD, we are able to calculate the fraction of a sample that is in each respective solid phase. Figure 7 shows the mass fraction of each phase for individual DSC samples in the range 54−64 wt % HNO_3. Mass fraction of each phase in a sample is calculated using the following equation:

$$y_i = \frac{EM_i}{\Delta H_i^{\text{fus}} m_T} \quad (1)$$

where y_i is the mass fraction of species i, E is the energy of the transition as measured by the DSC, M_i is the molar mass of solid i, ΔH_i^{fus} is the molar enthalpy of fusion of species i, and m_T is the total mass of the sample, where i represents NAT, NAD, etc. In the figure, each set of columns represents a different sample run in the DSC. All possible solids did not appear in each sample as would be expected from the stochastic nature of crystallization. Also note there is more than one sample at some concentrations. NAT is the major phase between 54 and 60 wt %; at higher concentrations, NAD fractions become comparable to the fraction of NAT in each sample, and in two cases is the major phase (one at 62 wt % and one at 63 wt %). At compositions higher than 64 wt % NAD is often the major phase, but these are not plotted in the figure. Fractions for TNAN are shown in the plot, but they must be considered as upper limits because the melting peaks (exotherms) in the DSC thermograms were occurring (at least partially) concurrently with recrystallization (endotherms); thus the energy due to melting TNAN is higher than what we measured.

Our results are in agreement with aerosol studies that show NAD is a component of solids in aerosols near a composition of 3:1 H_2O:HNO_3[22,25] and is the major phase at compositions near 2:1 H_2O:HNO_3.[21−23,25,35] However, we do see NAD drop dramatically as a fraction of the sample from ∼0.20 at 57 wt % to <0.005 at 56 wt % and below. Also, in the experiments of Bertram et al.,[25] they show that under conditions where both NAT and NAD nucleate, NAT grows to become the major phase in aerosols at stratospheric temperatures, and our results show the same conclusion. We are unable to conclude whether our mass fraction results for intermediate compositions between NAT (53.8 wt %) and NAD (63.6 wt %) agree with those of Prenni et al.[21] who saw the formation of NAD exclusively at a temperature of 194 K and an experiment time of 91 min. However, they describe their spectra as that of "water-rich" NAD (which we have discussed above in comparison to our TNAN spectra). Aerosol chamber residence times did not allow them to detect changes in the IR spectra due to formation of

NAT, as seen by Barton et al.[22] in their experiments, which were performed at lower temperatures. We surmise that our results may be similar to those of Barton et al. for intermediate compositions assuming NAT and NAD are present in comparable amounts in their experiments.

Summary and Stratospheric Implications

The binary aqueous phase diagram of nitric acid has been investigated using differential scanning calorimetry and FTIR analysis of thin films. The thermodynamic stability region of nitric acid dihydrate has been clearly defined (63.6−78 wt % HNO_3) including its melting envelope (63.6−73 wt % HNO_3). Our results are not in agreement with those of Worsnop et al.[18] Our results are in qualitative agreement with those of Ji and Petit,[17] but in general, we find their melting temperatures too low throughout the NAT-NAD-NAM region. We have also found from DSC and IR experiments that NAD can form in solutions down to concentrations of ∼52 wt % HNO_3, but we have not detected formation of NAD at even lower concentrations (with a threshold detection limit of ∼50 ppm.) This is in agreement with various aerosol studies that see some NAD formation in aerosols with compositions as dilute as 54 wt % but generally at much lower temperatures. In our experiments, we saw only very minor amounts of NAD (fraction of sample by mass <0.005) at solution compositions between 52 and 56 wt % and more significant amounts (>0.20) at 57 wt % and higher. Therefore, our results agree qualitatively with aerosol experiments, but Barton et al.[22] and Bertram et al.[25] did not report their sensitivity to detecting solid phases in aerosols, so we are unable to conclude whether we agree with respect to the amount of NAD present. One difference between our experiments and those mentioned is the higher temperature of our experiments. Our higher temperatures allow much faster growth of crystals once a phase nucleates (as demonstrated by Bertram et al.); thus we do not observe the time difference between nucleation of NAD and NAT seen by Barton et al. Our results also agree with aerosol studies that NAD is the major phase for solutions of 2:1 H_2O:HNO_3. Experiments on aerosols with a composition of 2.5:1 H_2O:HNO_3 (58.3 wt %) have been performed by Prenni et al.[21] and Barton et al. In both experiments the formation of NAD was observed, though in the latter work the formation of NAT was also seen for both this composition and others more dilute in HNO_3.

For *equilibrium* conditions in the stratosphere, we conclude NAD should not form in PSCs because the HNO_3 concentrations would never be above ∼45 wt % in the particles.[36] However, it has been suggested that nonequilibrium conditions may exist[37,38] or almost always exist[39] in polar stratospheric regions with respect to stratospheric particles. However, even in these cases, the HNO_3 concentration has been calculated to reach 51 wt % HNO_3 (cooling and warming in lee waves at 6 K/h)[36] to 58 wt % HNO_3 (cooling and warming at 150 K/h).[37] Although it is possible to form NAD under these conditions on the basis of our results and those reported for aerosols, NAD may simply convert to the more thermodynamically stable NAT over time. This conclusion also coincides with recent field measurements where the appearance of large, solid particles is best explained as NAT.[10,11]

A new hydrate has been identified that undergoes a melt−recrystallization transition at ∼228 K. We have identified a unique peak in the IR that corresponds to this solid, but otherwise the IR spectrum is similar to NAD. We have assigned this hydrate a composition of $4HNO_3 \cdot 9H_2O$, tetrakis(nitric acid) nonahydrate (TNAN). The amount of this hydrate in the mixed solid seems to be small and was only observed above concentrations of 57 wt % HNO_3, which would imply it will not be a major phase present in PSC particles. We disagree with the results of Salcedo et al.[27] who interpret the transitions they see in 54 wt % HNO_3 droplets between 224 and 228 K to be a NAD transition. Though we did not see evidence for TNAN at this concentration in our experiments, we would assign the melting transition they observed to be the melting of TNAN. We also disagree with their interpretation of transitions at 231 K to be a NAD transition. We have assigned this transition to the eutectic melting of NAM in contact with NAT. In general, we do not see NAD transitions below ∼233 K. Because Salcedo et al. rely on phase transition temperatures to identify the solids present in their samples, our assignment of the transition temperatures raises questions regarding their results for the nucleation rates of NAD under various conditions. Recent modeling studies on nucleation in atmospheric aerosols that have based their work on these results may also have to be reviewed.[40]

Two other transitions have been observed, but the specific phase transitions they correspond to have not been identified. We have measured a transition at a temperature lower than that of the melting of NAM on the nitric acid-rich side of the melting envelope. However, the concentration of these solutions would be too high for stratospheric droplets. A very minor transition was seen on the water-rich side of the NAT melting envelope; however, in this case we feel the amount of solid in this phase would be so low as to be irrelevant in PSCs. Additionally, we have no experimental evidence for the higher hydrates of nitric acid indicated by either Pickering[13] or Worsnop et al.[18]

Acknowledgment. We gratefully acknowledge the assistance of Chanda Ciriacks who performed the scan rate measurements. We also acknowledge the helpful comments of anonymous reviewers. This work was supported by the NSF Atmospheric Chemistry program (ATM-9911451).

References and Notes

(1) Solomon, S. *Rev. Geophys*. **1988**, *26*, 131.
(2) Anderson, J. G.; Toohey, D. W.; Brune, W. H. *Science* **1991**, *251*, 39.
(3) Dessler, A. *The Chemistry and Physics of Stratospheric Ozone*; Academic Press: New York, 2000.
(4) Wayne, R. *Chemistry of Atmospheres*, 3rd ed.; Oxford University Press: Oxford, U.K., 2000.
(5) Poole, L. R.; McCormick, M. P. *J. Geophys. Res*. **1988**, *93*, 8423.
(6) Hamill, P.; Turco, R. P.; Toon, O. B. *J. Atmos. Chem*. **1988**, *7*, 287.
(7) Wofsy, S. C.; Salawitch, R. J.; McElroy, M. B. *J. Atmos. Sci*. **1990**, *47*, 2004.
(8) Molina, M. J.; Zhang, R.; Wooldridge, P. J.; McMahon, J.; Kim, J. E.; Chang, H. Y. A.; Beyer, K. D. *Science* **1993**, *261*, 1418.
(9) Beyer, K. D.; Seago, S. W.; Chang, H. Y.; Molina, M. J. *Geophys. Res. Lett.* **1994**, *21*, 871.
(10) Voigt, C.; Schreiner, J.; Kohlmann, A.; Zink, P.; Mauersberger, K.; Larsen, N.; Deshler, T.; Kroger, C.; Rosen, J.; Adriani, A.; Cairo, F.; Di Donfrancesco, G.; Viterbini, M.; Ovarlwz, J.; Ovarlez, H.; David, C.; Dornbrack, A. *Science* **2000**, *290*, 1756.
(11) Fahey, D. W.; Gao, R. S.; Carslaw, K. S.; Kettleborough, J.; Popp, P. J.; Northway, M. J.; Holecek, J. C.; Ciciora, S. C.; McLaughlin, R. J.; Thompson, T. L.; Winkler, R. H.; Baumgardner, D. G.; Gandrud, B.; Wennberg, P. O.; Dhaniyala, S.; McKinney, K.; Peter, T.; Salawitch, R. J.; Bui, T. P.; Elkins, J. W.; Webster, C. R.; Atlas, E. L.; Jost, H.; Wilson, J. C.; Herman, R. L.; Kleinbohl, A.; von Konig, M. *Science* **2001**, *291*, 1026.
(12) DeMore, W. B.; Sander, S. P.; Golden, D. M.; Hampson, R. F.; Kurylo, M. J.; Howard, C. J.; Ravishankara, A. R.; Kolb, C. E.; Molina, M. J. *Chemical Kinetics and Photochemical Data for Use in Stratospheric Modeling*; JPL Publication 97-4; JPL: Pasadena, CA, 1997.
(13) Pickering, S. U. *J. Chem. Soc*. **1893**, *63*, 436.
(14) Kuster, F. W.; Kremann, R. *Z. Anorg. Chem*. **1904**, *41*, 1, 1904.
(15) Ritzhaupt, G.; Devlin, J. P. *J. Phys. Chem*. **1991**, *95*, 90.
(16) Tolbert, M. A.; Middlebrook, A. M. *J. Geophys. Res*. **1990**, *95*, 22,423.

(17) Ji, K.; Petit, J. C. *C. R. Acad. Sci. Paris* **1993**, *316*, II, 1743.
(18) Worsnop, D. R.; Fox, L. E.; Zahniser, M. S.; Wofsy, S. C. *Science* **1993**, *259*, 71.
(19) Fox, L. E.; Worsnop, D. R.; Zahniser, M. S.; Wofsy, S. C. *Science* **1995**, *267*, 351.
(20) Tsias, A.; Prenni, A. J.; Carslaw, K. S.; Onasch, T. P.; Luo, B. P.; Tolbert, M. A.; Peter, T. *Geophys. Res. Lett.* **1997**, *24*, 2303.
(21) Prenni, A. J.; Onasch, T. B.; Tisdale, R. T.; Siefert, R. L.; Tolbert, M. A. *J. Geophys. Res.* **1998**, *103*, 28, 439.
(22) Barton, N.; Rowland, B.; Devlin, J. P. *J. Phys. Chem.* **1993**, *97*, 5848.
(23) Bertram, A. K.; Sloan, J. J. *J. Geophys. Res.* **1998**, *103*, 3553.
(24) Bertram, A. K.; Sloan, J. J. *J. Geophys. Res.* **1998**, *103*, 13,261.
(25) Bertram, A. K.; Dickens, D. B.; Sloan, J. J. *J. Geophys. Res.* **2000**, *105*, 9283.
(26) Salcedo, D.; Molina, L. T.; Molina, M. J. *Geophys. Res. Lett.* **2000**, *27*, 193.
(27) Salcedo, D.; Molina, L. T.; Molina, M. J. *J. Phys. Chem.* **2001**, *105*, 1433.
(28) Zhang, R.; Wooldridge, P. J.; Molina, M. J. *J. Phys. Chem.* **1993**, *97*, 8541.
(29) Lide, D. R., Ed. *CRC Handbook of Chemistry and Physics*, 74th ed.; CRC Press: Boca Raton, FL, 1993; pp 3-208, 3-351 and 6-58.
(30) Koehler, B. G.; Middlebrook, A. M.; Tolbert, M. A. *J. Geophys. Res.* **1992**, *97*, 8065.
(31) Schubnell, M. *J. Thermal Anal. Calorimetry* **2000**, *61*, 91.
(32) Forsythe, W. R.; Giauque, W. F. *J. Am. Chem. Soc.* **1942**, *64*, 48−61.
(33) Chang, H. Y. A.; Koop, T.; Molina, L. T.; Molina, M. J. *J. Phys. Chem.* **1999**, *103*, 2673.
(34) Potier, J.; Potier, A. *C. R. Acad. Sci. Paris* **1956**, *242*, 1474.
(35) Disselkamp, R. S.; Anthony, S. E.; Prenni, A. J.; Onasch, T. B.; Tolbert, M. A. *J. Phys. Chem.* **1996**, *100*, 9127.
(36) Carslaw, K. S.; Luo, B. P.; Clegg, S. L.; Peter, T.; Brimblecombe, P.; Crutzen, P. J. *Geophys. Res. Lett.* **1994**, *21*, 2479.
(37) Meilinger, S. K.; Koop, T.; Luo, B. P.; Huthwelker, T.; Carslaw, K. S.; Krieger, U.; Crutzen, P. J.; Peter, T. *Geophys. Res. Lett.* **1995**, *22*, 3031.
(38) Tsias, A.; Prenni, A. J.; Carslaw, K. S.; Onasch, T. P.; Luo, B. P.; Tolbert, M. A.; Peter, T. *Geophys. Res. Lett.* **1997**, *24*, 2303.
(39) Biele, J.; Tsias, A.; Luo, B. P.; Carslaw, K. S.; Neuber, R.; Beyerle, G.; Peter, T. *J. Geophys. Res.* **2001**, *106*, 22,991.
(40) Tabazadeh, A.; Jensen, E. J.; Toon, O. B.; Drdla, K.; Schoeberl, M. R. *Science* **2001**, *291*, 2591.
(41) Wooldridge, P. J.; Zhang, R.; Molina, M. J. *J. Geophys. Res.* **1995**, *100*, 1389.